Assimilated ozone from EOS-Aura: Evaluation of the tropopause region and tropospheric columns

Ivanka Stajner,[1,2,3] Krzysztof Wargan,[1,2] Steven Pawson,[2] Hiroo Hayashi,[2,4] Lang-Ping Chang,[1,2] Rynda C. Hudman,[5] Lucien Froidevaux,[6] Nathaniel Livesey,[6] Pieternel F. Levelt,[7] Anne M. Thompson,[8] David W. Tarasick,[9] René Stübi,[10] Signe Bech Andersen,[11] Margarita Yela,[12] Gert König-Langlo,[13] F. J. Schmidlin,[14] and Jacquelyn C. Witte[15]

Received 20 April 2007; revised 11 December 2007; accepted 17 January 2008; published 29 May 2008.

[1] Retrievals from the Microwave Limb Sounder (MLS) and the Ozone Monitoring Instrument (OMI) on EOS-Aura were included in the Goddard Earth Observing System version 4 (GEOS-4) ozone data assimilation system. The distribution and daily to seasonal evolution of ozone in the stratosphere and troposphere during 2005 are investigated. In the lower stratosphere, where dynamical processes dominate, comparisons with independent ozonesonde and Measurement of Ozone and Water Vapour by Airbus In-Service Aircraft (MOZAIC) data indicate mean agreement within 10%. In the troposphere, OMI and MLS provide constraints on the ozone column, but the ozone profile shape results from the parameterized ozone chemistry and the resolved and parameterized transport. Assimilation of OMI and MLS data improves tropospheric column estimates in the Atlantic region but leads to an overestimation in the tropical Pacific and an underestimation in the northern high and middle latitudes in winter and spring. Transport and data biases are considered in order to understand these discrepancies. Comparisons of assimilated tropospheric ozone columns with ozonesonde data reveal root-mean-square (RMS) differences of 2.9–7.2 Dobson units (DU), which are smaller than the model-sonde RMS differences of 3.2–8.7 DU. Four different definitions of the tropopause using temperature lapse rate, potential vorticity (PV), and isentropic surfaces or ozone isosurfaces are compared with respect to their global impact on the estimated tropospheric ozone column. The largest sensitivity in the tropospheric ozone column is found near the subtropical jet, where the ozone- or PV-determined tropopause typically lies below the lapse rate tropopause.

Citation: Stajner, I., et al. (2008), Assimilated ozone from EOS-Aura: Evaluation of the tropopause region and tropospheric columns, *J. Geophys. Res.*, *113*, D16S32, doi:10.1029/2007JD008863.

1. Introduction

[2] The assimilation of space-based ozone data is motivated by several factors, including the need to understand its distribution in the troposphere, where it is a pollutant, and in the upper troposphere–lower stratosphere (UTLS), where it has climate impacts. Knowledge of the global ozone distribution in the troposphere and in the UTLS has improved with time, but it remains hampered by the sparse in situ observation capability and the complexity of deducing it from space-based radiance observations. This paper presents analyses of the ozone distribution in the UTLS and of the tropospheric ozone column, obtained by assimilation of data from NASA's Earth Observing System (EOS) Aura satellite into a global ozone assimilation system. The work has three main foci: first, to examine characteristics of

[1]Science Applications International Corporation, Beltsville, Maryland, USA.
[2]Global Modeling and Assimilation Office, NASA Goddard Space Flight Center, Greenbelt, Maryland, USA.
[3]Now at Noblis, Incorporated, Falls Church, Virginia, USA.
[4]Goddard Earth Sciences and Technology Center, University of Maryland, Baltimore County, Baltimore, Maryland, USA.
[5]Atmospheric Chemistry Modeling Group, Harvard University, Cambridge, Massachusetts, USA.
[6]Jet Propulsion Laboratory, Pasadena, California, USA.
[7]Royal Dutch Meteorological Institute, De Bilt, Netherlands.
[8]Department of Meteorology, Pennsylvania State University, University Park, Pennsylvania, USA.
[9]Air Quality Research Division, Environment Canada, Downsview, Ontario, Canada.
[10]Aerological Station Payerne, MeteoSwiss, Payerne, Switzerland.
[11]Danish Meteorological Institute, Copenhagen, Denmark.
[12]Instituto Nacional de Tecnica Aeroespacial, Madrid, Spain.
[13]Alfred Wegener Institute for Polar and Marine Research, Bremerhaven, Germany.
[14]NASA GSFC, Wallops Flight Facility, Wallops Island, Virginia, USA.
[15]Science Systems and Applications Inc., Lanham, Maryland, USA.

Copyright 2008 by the American Geophysical Union.
0148-0227/08/2007JD008863

the ozone profile in the UTLS; second, to discuss sensitivity of the inferred tropospheric ozone to the definition of the tropopause; and third, to discuss the factors that lead to uncertainty in tropospheric ozone in the assimilation.

[3] A major motivation of the EOS-Aura mission is to provide trace gas observations for studies of air pollution and climate [*Schoeberl et al.*, 2006]. Complementary information is retrieved from different Aura instruments. For example, the Microwave Limb Sounder (MLS) provides ozone profile data down to the upper troposphere with vertical resolution of about 3 km. The Dutch-Finnish Ozone Monitoring Instrument (OMI) provides total ozone columns with the horizontal resolution of 13 km $\times$ 24 km at nadir. Interpretation of these data using chemistry and transport models (CTMs) allows quantification of the roles that different processes play in determining ozone distribution and evolution. Data assimilation provides a framework for combining Aura data with an ozone model in order to quantify how well the observations agree with the model, which represents our understanding of chemistry and dynamics. Data assimilation also provides a capability for monitoring of the error characteristics of the incoming satellite data, as demonstrated by *Stajner et al.* [2004] for the ozone data from the Total Ozone Mapping Spectrometer (TOMS) and the Solar Backscatter UltraViolet Instrument (SBUV).

[4] Profile information from limb sounders can be combined with the total-ozone retrievals from backscattered ultraviolet instruments to deduce tropospheric ozone. Building on a range of earlier studies, *Ziemke et al.* [2006] computed stratospheric ozone columns from EOS MLS profiles and subtracted these from OMI total-column ozone to compute tropospheric ozone columns (TOC). Such techniques are subject to uncertainty. Since TOC represents only about 10% of the total column, values inferred in this way are the residual of two much larger values, so they are very sensitive to errors in both the total column and the stratospheric column. The strong vertical gradient in ozone concentrations in the UTLS coupled with the large spatial variations in tropopause location leads to uncertainty in the separation between stratospheric and tropospheric ozone in the MLS data. Along with the ozone data errors, there is also uncertainty in the location of the tropopause, which will impact the determination of tropospheric ozone column. This uncertainty arises from two factors, namely errors in meteorological analyses and the lack of conformity in choice of tropopause definition ("thermal," "dynamical," or "chemical" [see *Holton et al.*, 1995]), as discussed in section 5.

[5] The method of *Ziemke et al.* [2006] produces TOC at the MLS measurement locations in the daylight, where OMI retrievals are available, and where it is not excessively cloudy because OMI retrievals in the cloudy scenes include only climatological information below clouds. Global maps of TOC can be produced by either time averaging or mapping. For instance, the monthly aggregate of TOC obtained by compositing the data along the MLS orbit track gives near-global coverage. While this is of some value for studies of climate, it is less useful for other applications such as air pollution monitoring. Daily maps can be produced by spatial interpolation between the orbits, but such geometrical techniques include no information about the dynamical structure of the atmosphere. More sophisticated mapping techniques can be applied to the data to infer global, high-frequency distributions of TOC. One such technique is trajectory mapping, in which concentrations observed in one location are distributed using trajectories computed from meteorological analyses. *Schoeberl et al.* [2007] used this technique to produce global TOC distributions from OMI and MLS data, showing that realistic structures can be obtained.

[6] Assimilation of ozone is another advanced method that has potential as a technique for producing TOC. In this technique, as in the work of *Schoeberl et al.* [2007], the atmospheric analyses obtained by assimilating many meteorological observations into a general circulation model (GCM) are used to constrain the transport of ozone to produce global, three-dimensional fields. Statistical analysis is used to combine these ozone fields with the MLS and OMI retrievals to produce global ozone analyses that are constrained by local data in and around the observation locations, and by the suite of observations from the recent past in locations where there is no new information. Assimilation bears some similarity to trajectory mapping in that analyzed winds are used to transport information. It differs in that this transport is done inside a global model rather than on trajectories. Additionally, the global model for ozone includes representations of photochemical production and loss, as well as transport by clouds and turbulence, none of which are accounted for in the trajectory technique. The assimilation step also provides a framework for combining model forecast and observation information, weighted by the specified model and observation errors.

[7] A number of earlier studies have used assimilation of ozone to infer its global (and regional) distributions. Assimilation of ozone profiles from either limb sounding [*Wargan et al.*, 2005; *Jackson*, 2007] or occultation instruments [*Stajner and Wargan*, 2004] can yield realistic ozone distributions in the lower stratosphere and inside the Antarctic vortex. *Lamarque et al.* [2002] assimilated TOMS ozone columns and the Upper Atmosphere Research Satellite (UARS) MLS data into a chemistry-transport model to obtain daily estimates of TOC, showing reasonable agreement compared to TOC computed from ozonesondes. Compared to a model-only run, assimilation of satellite data substantially decreased differences of tropospheric ozone columns against ozonesondes. The impact on TOC was limited because UARS MLS data did not extend to pressures higher than 100 hPa. There is also a strong impact of transport error near the tropopause [*Lamarque et al.*, 2002]. *Wargan et al.* [2005] demonstrated that Michelson Interferometer for Passive Atmospheric Sounding (MIPAS) data, which have some information content down to about 150 hPa, can help constrain TOC. The present study demonstrates that EOS-MLS data, which extend down to the upper troposphere, coupled with the reasonable transport in the Goddard Earth Observing System, Version 4 (GEOS-4) data assimilation system [*Pawson et al.*, 2007], do represent an advance in our ability to deduce TOC from space-based data.

[8] Following a description of the EOS-Aura data (section 2) and some details of the ozone assimilation system (section 3), this work focuses on three important issues. The first (section 4) is a presentation of the three-dimensional ozone structure in the UTLS, including com-

parisons with in situ observations and detailed examination of the vertical profiles in this region, which is important because the ability to represent the profile in the vicinity of the tropopause strongly impacts the realism of computed TOC. The second (section 5) is a sensitivity study of deduced TOC to the choice of tropopause definition: this is important, because differences of 1–2 km in tropopause altitude can yield differences of 10–20% in TOC, which is similar to uncertainties in TOC deduced by various different studies. The third (section 6) is a presentation of a sample of tropospheric ozone maps from the assimilation, comparisons with ozonesonde data, and a discussion about potential sources of uncertainty that arise from the retrievals, the model, and the assimilation process. Prospects for future studies, including improvements in the assimilation, are discussed after a presentation of conclusions in section 7.

2. Aura Data

[9] The Aura satellite flies in a Sun-synchronous orbit at 705 km altitude, at an inclination of 98°, with 1:45 P.M. ascending equator-crossing time. In this study ozone data from two Aura instruments are used: MLS and OMI.

[10] MLS measures limb radiances in the forward orbital direction [*Waters et al.*, 2006]. The standard ozone product from the 240 GHz retrievals is used in this study. Comparisons of this ozone product from version 1.5 retrievals with independent data from solar occultation instruments indicate agreement within 5% to 10%, with MLS ozone being slightly larger in the lower stratosphere and slightly smaller in the upper stratosphere [*Froidevaux et al.*, 2006]. The vertical resolution of MLS ozone varies from ~2.7 km between 0.2 and 147 hPa to ~4 km at 215 hPa. Ozone mixing ratios between 0.14 and 215 hPa, which have positive precision and an even value of the MLS status variable are used. The precision of the MLS data is flagged negative when there is a large influence of a priori information on the retrieval (estimated precision is larger than half of the a priori error). An odd value of the status variable means that the retrieval diverged, too few radiances were available for the retrieval, or some other anomalous instrument or retrieval behavior occurred [*Froidevaux et al.*, 2008].

[11] Ultraviolet and visible spectrometers on Dutch-Finnish OMI detect backscattered solar radiation across a 2600 km wide swath [*Levelt et al.*, 2006]. The ground pixel size at nadir is 13 km × 24 km, or 13 km × 48 km at wavelengths below 308 nm, in the nominal global measurement mode. Two total ozone products are retrieved from OMI radiance measurements. One uses a Differential Optical Absorption Spectroscopy (DOAS) algorithm [*Veefkind et al.*, 2006], in which takes advantage of hyperspectral capabilities of OMI. The slant column density is derived by fitting of an analytical function to the measured Earth radiance and solar irradiance data over a range of wavelengths. An air mass factor is used to convert the slant column density to the vertical column density, followed by a correction for the effects of the clouds. The DOAS O3 retrieval uses the cloud pressure retrieved from OMI measurements on the basis of a method that relates the amount of absorption by the O2-O2 collision complex near 477 nm to the cloud height [*Accareta et al.*, 2004]. The OMTO3 ozone product is based on the Version 8 TOMS retrieval algorithm, which uses just two wavelengths, one that is weakly absorbed by ozone and one that is strongly absorbed by ozone (P. K. Bhartia and C. W. Wellemeyer, OMI TOMS-V8 Total O3 Algorithm, Algorithm theoretical baseline document: OMI ozone products, vol. II, edited by P. K. Bhartia, ATBD-OMI-02, version 2.0, 2002, available at http://eospso.gsfc.nasa.gov/eos_homepage/for_scientists/atbd/docs/OMI/ATBD-OMI-02.pdf): this OMTO3 product is used here. *McPeters et al.* [2008] validated these OMI retrievals against an ensemble of data from well-calibrated ground stations, finding an offset of +0.36% and a standard deviation of 3.5% in a sample of over 30,000 OMTO3 retrievals. Offset of the OMI DOAS ozone (collection 2) is larger than 1% and exhibits an additional seasonal variation of ±2%. In order to rely on the information from measurements, rather than climatological below-cloud ozone columns in cloudy regions, two criteria were applied to the OMTO3 OMI data used in the assimilation: these were that data were flagged as "good" and that the reflectivity at 331 nm was lower than 15%.

3. GEOS-4 Ozone Data Assimilation System

[12] Ozone assimilation is based on the approach of *Stajner et al.* [2001], who used SBUV partial columns and TOMS total ozone columns in a system in which forecast ozone fields were computed using a transport model. This system was enhanced to include parameterized ozone chemistry [*Stajner et al.*, 2004] and to use on-line transport within the GCM [*Stajner et al.*, 2006]. Additional data types have also been included: improved representation of the lower stratospheric ozone from the assimilation of limb-sounder data was discussed by *Wargan et al.* [2005]. Improved agreement between observations and the model, for example, near 20 hPa, when using the Goddard Earth Observing System Version 4 (GEOS-4) meteorological fields (compared to prior GEOS systems) was discussed by *Stajner et al.* [2004].

[13] Two types of experiment were used in this study. The first were model runs, in which ozone was not constrained by observations. The second were assimilations, in which the model provided the background fields for statistical analyses. In both types of experiment, the transport and chemistry were constrained by identical meteorological fields and chemical source-sink mechanisms. All the runs were integrated through 2005 starting from a common initial ozone field on 31 December 2004, which was obtained from an assimilation run that started in August 2004.

3.1. Model

[14] Ozone forecasts are computed using the Goddard Earth Observing System Version 4.0.3 (GEOS-4) GCM. The GCM includes flux-form semi-Lagrangian transport on quasi-Lagrangian levels [*Lin and Rood*, 1996; *Lin*, 2004]. It was run at a resolution of 1.25° longitude by 1° latitude with 55 layers between the surface and 0.01 hPa. Every 6 hours meteorological variables in the GCM are reinitialized to those from the GEOS-4.0.3 meteorological assimilation [*Bloom et al.*, 2005]. We use 6-hourly averages of assimilated meteorological fields, rather than instantaneous

analyses, to reinitialize the GCM in order to filter high-frequency transients and hence improve the transport characteristics [*Pawson et al.*, 2007]. The residual circulation in this constrained GCM is about 30% faster than in reality. Because the ozone assimilation is performed after the meteorological assimilation is complete, there is no feedback of ozone into the radiation module of the GCM.

[15] For the present work, a parameterized representation of ozone chemistry was implemented in the GCM, updated from *Stajner et al.* [2006]. Zonal-mean production rates (P) and loss frequencies (L) for stratospheric gas-phase chemistry are based on the work of *Douglass et al.* [1996]. At pressures lower than 10 hPa, P was adjusted so that the equilibrium ozone distribution agrees with the Upper Atmosphere Research Satellite (UARS) reference climatology, on the basis of 7 years of UARS MLS and Halogen Occultation Experiment data. To represent polar ozone loss, a parameterization for heterogeneous ozone chemistry is included using the "cold tracer," which was used to study the impact of interannual meteorological variability on ozone in middle latitudes [*Hadjinicolaou et al.*, 1997] and in the assimilation of ozone data [*Eskes et al.*, 2003]. This tracer mimics chlorine activation at low temperatures in the polar winter stratosphere. The cold tracer is advected, and its presence under sunlight leads to the ozone loss of 5% per day when the cold tracer is fully activated. Although this scheme does not account for the full complexity of the heterogeneous chemistry leading to the ozone loss, it can in principle capture some of the interannual variability and the zonal asymmetry of ozone loss triggered by low temperatures in and around the polar vortex.

[16] To calculate tropospheric ozone, 24-hour mean P, L, and deposition rates derived from an integration of the GEOS-Chem model (version 7.04) were included. The GEOS-Chem model was driven by GEOS-4 meteorological fields, at native GEOS-4 levels, but at $2° \times 2.5°$ horizontal resolution. Because of the rapid, emission- and weather-related variations in tropospheric ozone chemistry, P, L and deposition rates were updated daily, so they are specific to each day of 2005, including effects of synoptic-scale variability (e.g., stagnation events, uplift from local convection, isentropic lifting in synoptic storms). GEOS-Chem provides a global simulation of ozone-NO_x-hydrocarbon-aerosol chemistry with 120 species simulated explicitly. A general description of GEOS-Chem is given by *Bey et al.* [2001] and a description of the coupled oxidant-aerosol simulation as used here by *Park et al.* [2004]. Anthropogenic emissions over the United States use EPA National Emission Inventory for year 1999 (NEI99). The NEI99 NOx sources from power plants have been reduced by 50% during the ozone season and CO sources by 50% following *Hudman et al.* [2007] as constrained by observations during the International Consortium on Atmospheric Transport and Transformation (ICARTT) aircraft study. Outside of the United States we use a global anthropogenic inventory for year 1998, as described by *Bey et al.* [2001]. For biomass-burning emissions, climatological means are redistributed according to MODIS fire counts [*Duncan et al.*, 2003]. The lightning source of NO_x in GEOS-Chem is computed locally in deep convection events with the scheme of *Price and Rind* [1992] that relates number of flashes to convective cloud top heights, and the vertical distribution from *Pickering et al.* [1992]. Regional adjustments to lightning flashes are applied using a climatology of lightning flash counts based on observations from the Optical Transient Detector and the Lightning Imaging Sensor.

[17] Three experiments had been performed for this work. The first one is a run of the model that used the boundary conditions and chemical approximation described above. It used the GEOS-4 meteorological analyses, as in the work of *Pawson et al.* [2007]. This is equivalent to a CTM integration performed on line in the GEOS-4 GCM, because the ozone does not feed back to the models radiation code. Two other assimilation experiments are introduced below, at the end of section 3.2.

3.2. Statistical Analysis

[18] Aura data are assimilated every 3 hours using a sequential statistical analysis method. Differences between Aura data within the 3-hour window centered at the analysis time and the model forecast valid for the analysis time are computed. These are observed-minus-forecast (O-F) residuals. Statistical analysis based on the Physical-space Statistical Analysis Scheme [*Cohn et al.*, 1998] is used to compute the analyzed ozone from the model forecast and the O-F residuals based on specified observation error covariances, forecast error covariances, and the observation operator, which maps the model space to observed variables. Statistical analysis uses a univariate scheme that was developed by *Stajner et al.* [2001] for nadir-sounding data, with an observation model using bilinear horizontal interpolation (using four bracketing model profiles) of ozone mixing ratio profiles to the measurement location, followed by vertical integration to obtain total or partial ozone columns. *Wargan et al.* [2005] adapted this scheme to include limb-sounder retrievals from the Michelson Interferometer for Passive Atmospheric Sounding (MIPAS), using the same bilinear horizontal interpolation but with linear interpolation in logarithm of pressure between model levels.

[19] The forecast error correlation model from *Stajner et al.* [2001] is used, but the horizontal forecast error length scale is reduced to 250 km. This is motivated by desire to represent, rather than smooth out, tropospheric ozone features and by the following improvements in the assimilation system: higher model resolution, improved stratospheric transport, and inclusion of chemical parameterizations. Experimentation with three length scales, L = 150, 250 and 400 km, showed that the lowest root-mean-square (RMS) of OMI O-F residuals is for L = 400 km in the tropics (~5.5 Dobson Units, DU) and for L = 150 km from 60°N to 80°N (~7 DU) during September 2004. Even though the correlation model is anisotropic, with longer zonal length scale in the tropics, these experiments indicate that an even stronger degree of anisotropy may be beneficial. Global RMS of OMI O-F residuals is ~7.2 DU for L = 150 km and ~6.6 DU for L = 250 and 400 km, which is ~2.3% of the OMI observed total ozone.

[20] The forecast error variances are specified to be proportional to the ozone field, and the constant of proportionality is reduced by 50% in the regions (mainly the troposphere) where the ozone mixing ratio is less than 0.1 ppmv. This reduction was motivated by the finding of

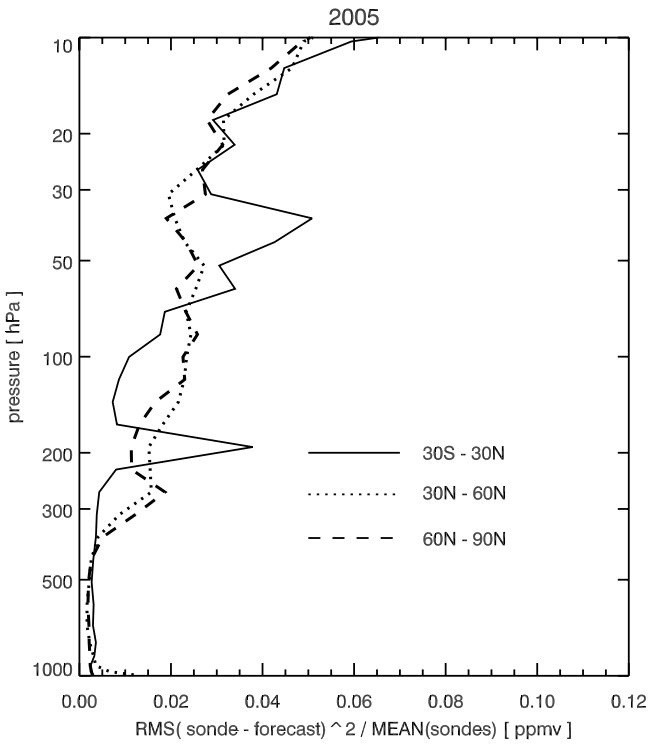

Figure 1. The ratio of the mean square difference between ozonesonde observations and forecasts from Aura assimilation divided by the mean of the sondes is shown for the tropics (solid), northern middle latitudes (dotted), and northern high latitudes (dashed) for year 2005.

Stajner et al. [2001] that the proxy for the ratio between forecast error variance and the ozone field increases at the tropopause and is higher in the stratosphere than in the troposphere. Using assimilation of Aura data we again found that the mean square difference between ozonesondes and the ozone forecasts divided by the mean of the ozonesondes is lower in the troposphere than in the stratosphere (Figure 1). Note that the large value of this ratio at 191 hPa in the tropics is eliminated (falling below 0.005 ppmv) when the computation is restricted to those profiles with ozone lower than 0.1 ppmv at 191 hPa. The increase in the ratio near 40 hPa in the tropics may be related to the change in the ozone profile due to the phase of the Quasi-Biennial Oscillation (QBO) [*Logan et al.*, 2003]. Vertical wind shear due to the QBO is not reproduced well in GEOS-4 operational runs that are used here, which do not employ a highly anisotropic, nonseparable forecast error correlation model developed by *Gaspari et al.* [2006].

[21] Observation errors are modeled as uncorrelated. The standard deviation of MLS observation errors used in the assimilation typically increases with decreasing pressure: from ~0.15 ppmv at 215 hPa, over ~0.4 ppmv at 14.7 hPa, to ~0.6 ppmv at 0.14 hPa. These errors are larger than the MLS retrieval precision, which varies from about 2% to 15% in the middle stratosphere. The profile of observation error standard deviation that is used in the assimilation has a similar shape, but larger magnitude than the profile of the aggregate of precision and accuracy estimates for MLS version 2.2 data [*Froidevaux et al.*, 2008]. The larger magnitude is consistent with larger biases in version 1.5 data that are used here. OMI data were averaged onto 2° × 2.5° grid prior to assimilation in order to reduce the data volume and potentially improve data precision. As only cloud-free OMI data are used, the number of OMI data per grid box has a nonuniform distribution with the mode of 2 and mean of 33 observations per grid box. These averaged OMI data are assimilated with the error standard deviation specified as 2%. Individual OMI observations have error standard deviation of 3.5% (section 2). Averaging of about 33 OMI observations would reduce the standard deviation to $3.5/\sqrt{33} = 0.61\%$ if the errors are independent, or remain at 3.5% if the errors are perfectly correlated. Including the bias of 0.4% (section 2), the RMS of the error of the OMI average is between 0.73% and 3.52%. Given that some of the OMI errors within a 2° × 2.5° box are correlated, for example, owing to common climatological assumptions used in the retrievals, the chosen error of 2% for the OMI box averages is plausible.

[22] Three experiments are presented in comparisons. The main Aura assimilation experiment that is evaluated here uses the statistics defined in this section. Two additional experiments are: a perturbation experiment in which MLS observation errors are reduced by 50% (in section 6 only), and a model run (described in section 3.1) that does not assimilate any Aura data.

4. Ozone in the Upper Troposphere and Lower Stratosphere

[23] This section discusses the representation of ozone structures in the UTLS of the analyses. This is important, because ozone mixing ratios increase rapidly from tropospheric values (<0.1 ppmv) to stratospheric values (often larger than 1 ppmv) over a thin layer. Spatial variations in tropopause height lead to similar structure in horizontal distributions of ozone. Accurate representation of these gradients and their location relative to the tropopause is thus an important factor in computing the TOC. Furthermore, estimates of stratosphere-troposphere exchange (STE) of ozone depend on accurate representation of the spatial gradients. Errors in model vertical transport, such as excessive downwelling, become evident as biased ozone in the UTLS. Examples of validation of the assimilated Aura ozone in the UTLS against independent sonde and aircraft data are presented.

[24] *Stajner et al.* [2001] showed that assimilation of SBUV and TOMS ozone did not accurately constrain the profile shape in the UTLS, with a pronounced (~30%) overestimation of ozone concentrations near 150 hPa. This was owing to the lack of constraint on ozone profiles in this region and a poor representation of transport in that analysis. Assimilation of ozone from the limb-sounding MIPAS instrument reduced systematic errors in the lower stratosphere [*Wargan et al.*, 2005]. Figure 2a shows that the systematic errors of the assimilated Aura ozone are small compared to independent ozonesonde data in northern middle and high latitudes (30°N–90°N). Mean differences between sonde measurements and collocated ozone profiles in January and February 2005 are less than ±10% between 10 and 500 hPa. This improvement over the work of *Stajner et al.* [2001] is due to improved transport in the present

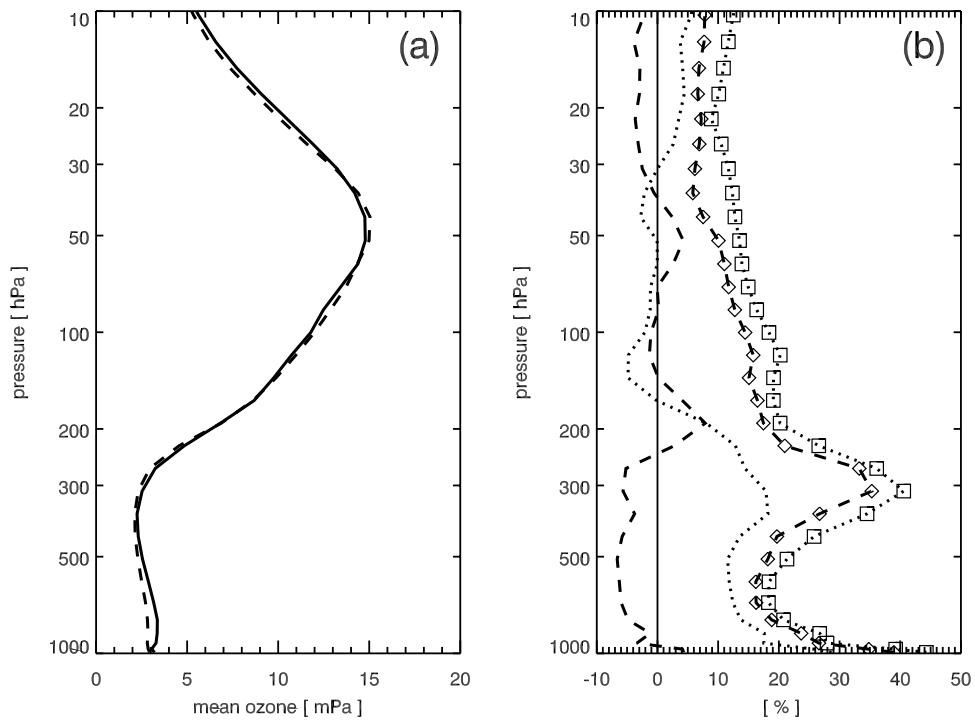

Figure 2. (a) Mean of sonde profiles (solid) and collocated ozone profiles from assimilation of Aura data (dashed) for 282 soundings north of 30°N in January and February 2005. (b) Mean difference relative to the mean of sondes between Aura assimilation and sondes (dashed) and between the model run and sondes (dotted). The RMS differences between the Aura assimilation and the sondes (diamonds) and the RMS differences between the model run and the sondes (squares) relative to the sonde mean are shown. Profiles from 294 soundings north of 30°N in March, April, and May 2005 were used. Sonde data for both comparisons were obtained from the Aura Validation Data Center and the Envisat Calibration and Validation database.

system [*Pawson et al.*, 2007] and to the assimilation of Aura data. The latter is evident from the comparison of the model simulation using the same meteorological fields (without the assimilation of Aura data) with the ozonesondes, and Aura assimilated ozone in the same region during March, April, and May 2005 (Figure 2b). Ozone in the UTLS is overestimated in the model fields (by 19% near 300 hPa), in comparison to the ozonesondes. In contrast, assimilation of the Aura data brings the mean ozone to within 8% of the mean sonde profiles between the surface and 10 hPa. Further comparisons focusing on the lower stratosphere (not shown) with all available ozonesondes in January to June in the tropics (30°S–30°N), northern middle latitudes (30°N–60°N), and northern high latitudes (60°N–90°N) revealed mean differences within 10% in each region at pressures between 50 and 200 hPa.

[25] Independent validation data are available from the Measurement of Ozone and Water Vapour by Airbus In-Service Aircraft (MOZAIC) program [*Marenco et al.*, 1998; *Thouret et al.*, 1998a]. Sensors onboard several commercial aircraft measure ozone concentrations, mostly at cruising altitudes in the UTLS [*Thouret et al.*, 1998b]. An example of a MOZAIC flight path from Charlotte, North Carolina, to Munich, Germany, is shown in Figure 3a. The assimilated Aura ozone along this flight shows good representation of larger-scale variability, as the flight encountered higher stratospheric values and lower tropospheric values (Figure 3b).

[26] Histograms of differences between MOZAIC data at and above 8 km altitude and collocated Aura analyses have a Laplace-like (or double exponential-like) distribution. This is illustrated by the example for July 2005 in Figure 4, which shows the distribution of probability of MOZAIC-minus-assimilation differences (black line). The distribution is sharply peaked at the mode, with a rapid drop-off close to the mode, but with extended "tails." The mode of the distribution is slightly negative (assimilated values are biased high). The data have been separated into four groups on the basis of MOZAIC and assimilated ozone each being lower than or exceeding 0.1 ppmv, which typically delineates between tropospheric and stratospheric ozone. This separation reveals that most of the small MOZAIC-assimilation differences occur when both MOZAIC and assimilation have tropospheric ozone values (<0.1 ppmv; green line). The largest contribution to the "tails" of the distribution comes from the measurements for which MOZAIC and assimilation both have stratospheric ozone values (≥0.1 ppmv; yellow line). Note also that the peak stratospheric ozone differences occur close to the zero line, indicating that the MLS data lead to a very high-quality global assimilation. The mode of the tropospheric differences is slightly negative, leading to the negative offset in the total histogram, indicating that

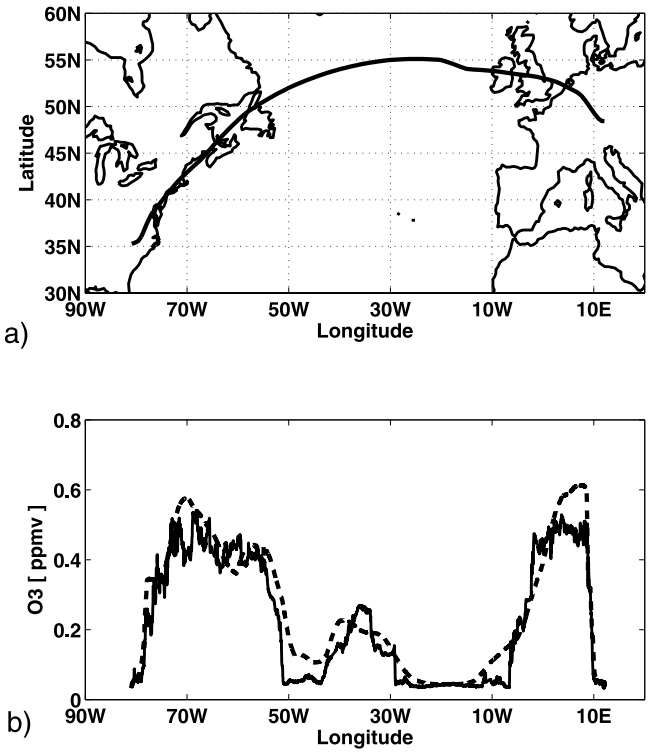

Figure 3. (a) A map of the Measurement of Ozone and Water Vapour by Airbus In-Service Aircraft (MOZAIC) flight on 19 February 2005 from Charlotte, North Carolina, to Munich, Germany. (b) MOZAIC-measured ozone along this flight (solid) and collocated ozone from the assimilation of Aura data (dashed).

tropospheric ozone values near the tropopause in the assimilation are biased high compared to the MOZAIC data.

[27] Laplace-like distributions were seen in the analysis of ozone data along flight tracks of research aircraft in comparisons of measurements offset by a fixed distance [*Sparling and Bacmeister*, 2001]. They found this type of distribution for all but very short distances (which are more impacted by correlated instrument noise). We found that the distribution of MOZAIC-minus-assimilated differences is comparable to along-track differences of MOZAIC measurements offset by ~400 km. This is close to the distance between four model grid points along the latitude circle in middle latitudes, which is arguably the finest scale that is represented in the grid-point model. For example, about six grid points are needed to represent the discontinuity on one side of a square wave using flux-form semi-Lagrangian piecewise parabolic method [see *Lin and Rood*, 1996, Figure 4].

[28] Mean differences between analyses and MOZAIC data at and above 8 km altitude were evaluated for each month from January to August 2005 (not shown). They range from ~−4% in January, over ~1% in February, ~5% in April and June, ~6% in March, July, and August, to ~10% in May. Note that this indicates that the close agreement between analysis and MOZAIC mean values in July seen in Figure 4 is representative of the whole period of comparison.

[29] The quality of stratospheric ozone columns in the Aura assimilation is evaluated by comparisons with the Stratospheric Aerosol and Gas Experiment (SAGE) II data. Ozone profiles that are retrieved from SAGE II solar occultation measurements, with a vertical resolution of about 1 km, have been extensively evaluated [e.g., *Wang*

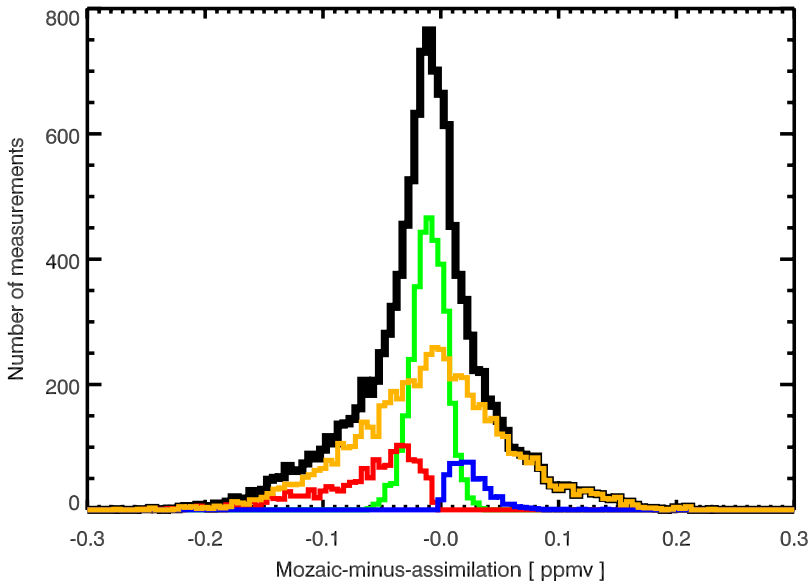

Figure 4. Histogram of the differences between MOZAIC and collocated ozone from the Aura assimilation for all MOZAIC measurements at and above 8 km altitude in July 2005 (black). The data were divided into four subsets based on MOZAIC (M) and assimilation (A) ozone values in ppmv: M, A < 0.1 (green), M < 0.1 ≤ A (red), A < 0.1 ≤ M (blue), and M, A ≥ 0.1 (yellow). The bin width is 0.005 ppmv. Prior to comparisons, MOZAIC data were averaged onto a 1° × 1.25° grid, which is the resolution of the Aura assimilation.

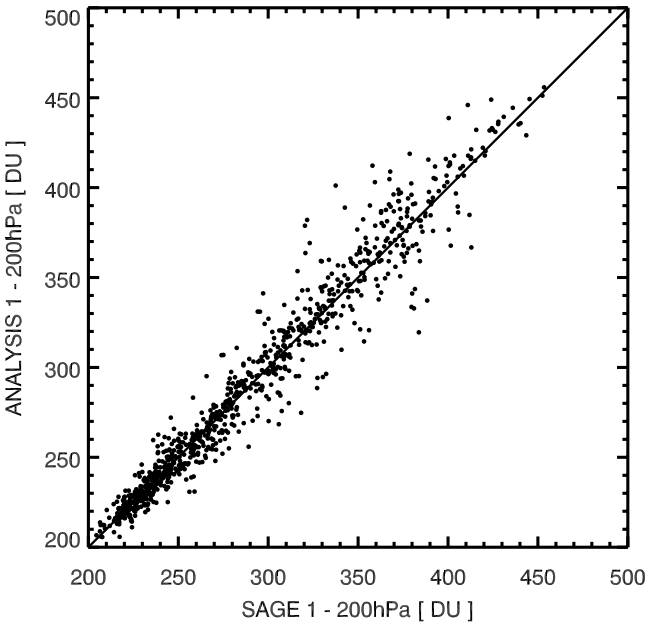

Figure 5. Ozone partial column between 1 and 200 hPa from Stratospheric Aerosol and Gas Experiment II (SAGE II) and collocated Aura assimilation profiles for January to March 2005.

et al., 2002]. SAGE version 6.20 data for January to March 2005 are used here. The scatterplot comparing partial ozone columns between 1 and 200 hPa from SAGE II and the collocated Aura assimilation is shown in Figure 5. A close agreement is seen between the two data sets over a wide dynamic range from 200 to 450 DU. The statistics of the differences (Table 1) show excellent agreement in the mean columns and the RMS differences that are within 5%.

[30] Comparisons with ozonesondes and MOZAIC data indicate that assimilated Aura ozone data have small systematic errors compared to in situ data, which makes the assimilated Aura data credible for studies of the ozone distribution around the tropopause. The stratospheric ozone columns from Aura assimilation were shown to be in excellent agreement with SAGE II data.

5. Derived Tropospheric Ozone: Impact of Different Tropopause Definitions

[31] In this section, the TOC from the assimilated data is examined. The TOC in Dobson Units (1 DU = 2.69 10^{16} molecules cm^{-2}) is given by

$$0.7891 \int_{pt}^{ps} \mu \cdot dp, \tag{1}$$

where μ is the ozone mixing ratio in ppmv, p is pressure, pt is pressure of the chosen tropopause, ps is the surface pressure (all pressures are in hPa). As discussed in section 1, the information from observations that contributes to this product is limited to the stratospheric and upper tropospheric profile (from MLS) and the total ozone column (from OMI). Apart from the quality of the stratospheric ozone analyses and the total column information, two other factors impact the determination of TOC. These are the definition of the tropopause and the accuracy with which it can be located.

[32] *Ziemke et al.* [2006] used the tropopause height determined from the lapse rate in NCEP-NCAR reanalyses [*Kistler et al.*, 2001]. *Birner et al.* [2006] found that the extratropical tropopause is too low and too warm in these analyses, consistent with results of *Schoeberl* [2004] from other analyses. This uncertainty will result in an underestimation of TOC. This aspect is not considered in this study, but remains an important caveat in the estimations of TOC.

[33] Early comparisons of several TOC products derived from EOS-Aura data suggested that some of the differences might be due to the choice of tropopause (G. Morris, personal communication, 2006). *Schoeberl et al.* [2007] avoid this issue by comparing ozone columns between the surface and 200 hPa. This approach removes the sensitivity to choice of tropopause, but it does not separate the tropospheric from the stratospheric ozone.

[34] There are valid reasons for using any of at least three different tropopause definitions [e.g., *Holton et al.*, 1995]. In the WMO "thermal" definition, the tropopause is the lower boundary of a layer in which temperature lapse rate is less than 2 K km^{-1} for a depth of at least 2 km. Even though this definition can be applied to a single temperature profile from a sounding or a model, it is not uniquely defined when multiple stable layers are present (especially in the vicinity of the subtropical jet). The "dynamical" definition of the tropopause relies on the increase in the potential vorticity (PV) from low values in the troposphere to higher values in the stratosphere. This definition offers an advantage over the thermal definition in that it is determined by the three-dimensional motion of air, which provides a more faithful representation of the tropopause evolution during the passage of wave disturbances. Even with this definition, various PV isopleths (ranging between 1 and 4 PVU) have been applied to define the tropopause from three-dimensional meteorological fields [e.g., *Hoerling et al.*, 1991]. A third way of defining the tropopause results from changes in the chemical composition of air at the tropopause. For example, stratospheric air is rich in ozone, but has less carbon monoxide and water vapor than the tropospheric air. A "chemical" definition of the tropopause relies on values of a constituent, or its vertical gradient, exceeding a specified threshold [*Bethan et al.*, 1996]. High-resolution measurements of constituents near the tropopause support the notion of a tropopause layer in which the transition of the chemical composition occurs over a couple of kilometers or more, rather than at a single tropopause surface [*Pan et al.*, 2004; *Zahn et al.*, 2000].

Table 1. Statistics of SAGE II–Minus–Aura Assimilation Differences in the Ozone Columns Between 1 and 200 hPa

Region	Number of SAGE II Profiles	Mean Difference, Percent	RMS Difference, Percent
90°S–60°S	40	−1.84	2.43
60°S–30°S	140	−0.55	3.27
30°S–30°N	217	0.49	2.62
30°N–60°N	358	−0.01	5.00
60°N–90°N	174	−1.06	4.49

Table 2. The Four Tropopause Definitions Used, the Criterion Used for Each Definition, Together With the Pressure Range Over Which It Is Applied, and the Notation for the Tropospheric Ozone Column Computed by Integrating Assimilated Ozone Between the Surface and the Tropopause Using Each Definition

Tropopause Definition Name	Criterion	Search Range, hPa	Tropospheric Ozone Column Notation
WMO (algorithm by *Reichler et al.* [2003])	lower boundary of at least 2 km thick layer in which lapse rate <2 K km^{-1}	550–75	Ω_{WMO}
Dynamical	lower of |PV| = 3.5 PVU or θ = 380 K	<600	Ω_D
Ozone	ozone = 0.1 ppmv	<500	Ω_O
Ozone from above	ozone = 0.1 ppmv	>51	Ω_{OA}

[35] Here, the assimilated global ozone distributions are used to investigate sensitivity of TOC to the definition of the tropopause. This exploits the availability of time-dependent, three-dimensional ozone concentrations in the analyses in a way that is not possible with more traditional TOC estimation methods [e.g., *Ziemke et al.*, 2006]. Four tropopause definitions (Table 2) will be used in this sensitivity study. GEOS-4 meteorological fields are used to determine the WMO and dynamical tropopauses. Assimilated Aura ozone data are used to determine ozone tropopause (searching for 0.1 ppmv in the profiles from below, i.e., starting at 500 hPa and proceeding toward higher altitude) and "ozone tropopause from above" where 0.1 ppmv is found by the search from above, which begins near 51 hPa and proceeds downward toward the surface. Comparisons of the tropopauses according to WMO and dynamical definitions have been made in global models and assimilated fields [e.g., *Hoerling et al.*, 1991]. Comparisons of tropopause defined according to WMO and ozone definitions are possible from in situ measurements from ozonesondes and research or commercial aircraft [*Bethan et al.*, 1996; *Pan et al.*, 2004; *Zahn et al.*, 2000]. Such comparisons can be made for the global ozone distribution in the assimilated data. Differences in the position of the tropopause according to these definitions may provide an indication of the thickness of the tropopause layer over which air characteristics change from tropospheric to stratospheric.

[36] A comparison of the zonal mean tropopause computed in four ways on 15 February 2005 (Figure 6a) reveals broad similarity in its shape: its altitude varies from 7 km near the poles to 17 km in the tropics, with particularly large meridional gradients near 30°N. In the northern middle latitudes, the WMO tropopause is about 0.7 to 1 km higher than the ozone tropopause. This is consistent with findings from European [*Bethan et al.*, 1996] and North American [*Thompson et al.*, 2007b] ozonesonde data. The ozone tropopause and the dynamical tropopause agree closely between 60°S and 30°N and north of 75°N. A higher ozone tropopause over the southern polar region may be due to model errors, such as excessive upwelling, below the altitude constrained by the MLS data. The WMO tropopause is anomalously high over the North Pole in this example. In the vicinity of the subtropical jet the ozone tropopause is the lowest, and this is the only region with substantial differences in ozone tropopause from above and below. This indicates frequent profiles in which 0.1 ppmv of ozone is found above higher ozone values, as can occur when isentropic transport brings upper tropospheric ozone-poor air over ozone-richer air in the lowermost stratosphere in middle latitudes.

[37] The impacts of different tropopause definitions on the computed tropospheric ozone column are shown in Figure 6b. Even though the various definitions lead to 0.5–1 km tropopause height differences in the tropics, the tropospheric ozone columns agree very closely. This is due to the high altitude of tropopause surfaces, relatively small changes in the pressure, low ozone mixing ratios (lower than 0.1 ppmv because the ozone tropopause is the highest), and consequently small differences in the ozone column between any two tropopause surfaces. Larger differences in tropospheric columns are seen near 30°S and north of 20°N. The tropospheric column using WMO definition, Ω_{WMO}, is typically the highest and that using ozone definition, Ω_O, is lower by about 2–3 DU or 10%. An extreme difference in this example is seen at the North Pole, where the tropo-

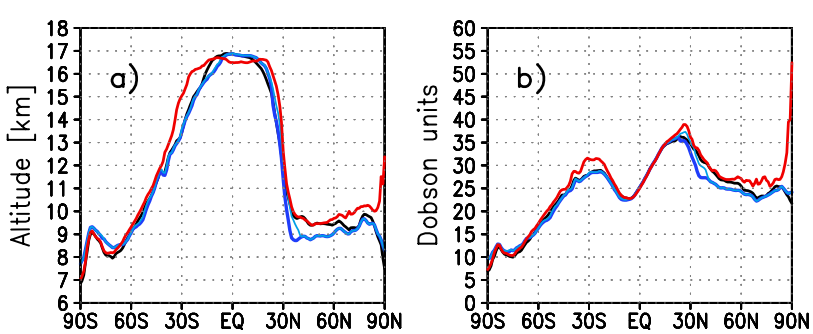

Figure 6. (a) Zonal mean altitude of the tropopause at 0000 UT, 15 February 2005, for four definitions in Table 2: World Meteorological Organization (WMO) (red), dynamical (black), ozone (blue), and ozone from above (light blue). (b) Corresponding zonal mean tropospheric columns Ω_{WMO} (red), Ω_D (black), Ω_O (blue), and Ω_{OA} (light blue).

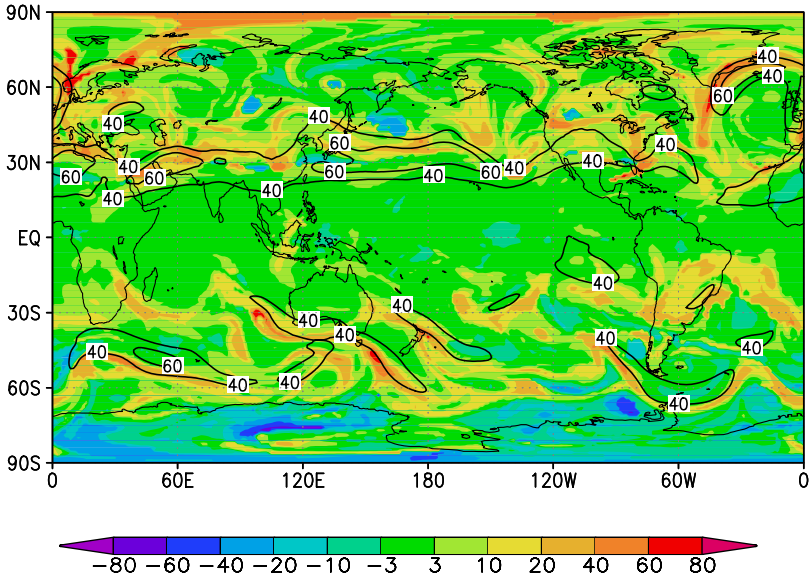

Figure 7. Relative difference between WMO-defined and ozone-defined tropospheric ozone columns, $(\Omega_{WMO} - \Omega_O)/\Omega_{WMO}$, in percent (color) for 0000 UT on 15 February 2005. Wind magnitude at 200 hPa is shown by 40 and 60 m/s contours.

spheric ozone columns by other definitions are about 50% lower than Ω_{WMO}.

[38] A map of differences between tropospheric ozone columns defined using WMO and ozone definitions relative to the WMO-defined column, $(\Omega_{WMO} - \Omega_O)/\Omega_{WMO}$, for 15 February is shown in Figure 7. Coherent "streamers" of larger positive differences are seen, especially near 30°N, extending over northern Atlantic and northern Europe, toward the North Pole. Similar streamers are seen in the southern middle latitudes. The wind magnitude at 200 hPa is shown by contours. Many of the larger differences are located on the poleward side of the strongest wind jets in the UTLS.

[39] Comparisons of tropospheric ozone columns show that monthly means of Ω_O, $\Omega_{OA,}$ and Ω_D differ by less than 3 DU south of 25°N in February and July 2005 (Figure 8). The largest differences $\Omega_{WMO} - \Omega_O$, $\Omega_D - \Omega_O$, and $\Omega_{OA} - \Omega_O$ are seen near the northern subtropical jet, with differences typically largest for Ω_{WMO}, and smallest for Ω_{OA}. The differences against Ω_O north of 25°N are larger in July (up to 20 DU for Ω_{WMO}) than in February (up to 12 DU for Ω_D). There is a pronounced zonal asymmetry in July, when largest differences between other tropospheric columns and Ω_O are seen over Asia, extending from the Mediterranean to Japan. During August to October, the differences weaken in the northern and strengthen in southern middle latitudes (not shown). A zonal asymmetry develops, with larger differences near Australia, which are starting to appear in $\Omega_D - \Omega_O$ in July. This is believed to be related to the dynamical conditions leading to accumulation and subsidence of stratospheric ozone to the south of Australia and increase in the ozone mixing ratio below the dynamical tropopause.

[40] Focusing on a small European region (50°N–80°N, 0°E–20°E) during fall and winter months in 2005, we examine the distribution of $(\Omega_{WMO} - \Omega_O)/\Omega_{WMO}$. This is chosen to allow comparison with the results of *Bethan et al.* [1996], who used sonde measurements within this region, mostly in fall and winter months. The distribution from Aura assimilation (Figure 9) resembles their findings from sondes [*Bethan et al.*, 1996]. Even though in ~1/4 of the cases Ω_O is higher than Ω_{WMO} by less than 5%, for ~2/3 of the cases, Ω_O is lower than Ω_{WMO}, occasionally by more than 80%. In the Aura assimilation for 2005 the latter cases occur in February, when strong winds are seen in the UTLS region in the Northern Atlantic, approaching Northern Europe. This is consistent with findings of *Bethan et al.* [1996] that the largest differences between Ω_{WMO} and Ω_O are found on the cyclonic side of strong jets in profiles with "indefinite thermal tropopause." They use this term for profiles in which lapse rate changes slowly from typical tropospheric to stratospheric values over several km thick layers. Large differences are not confined to winter: an example of ozonesonde profile with the WMO tropopause higher than the ozone tropopause by 6.9 km and Ω_O lower than Ω_{WMO}, by 56% was presented by *Thompson et al.* [2007b].

[41] Quantitative comparisons of tropospheric ozone columns Ω_{WMO}, Ω_D, Ω_O, and Ω_{OA} indicate substantial differences: from ~10% on average in northern middle latitudes in the winter, over monthly-mean differences of ~30% in parts of Asia in July, to cases with differences of ~80% on the poleward side of strong wind jets in the UTLS.

6. Tropospheric Ozone

[42] Tropospheric ozone time series are shown in Figure 10 for Sodankyla in the northern high latitudes (67°N), for Payern in the northern middle latitudes (47°N), and for Nairobi in the tropics (1°S) [*Thompson et al.*, 2003], which are all within 30° longitude (7°E–37°E). For these comparisons the tropopause is determined using WMO definition applied to the ozonesonde temperature profiles. This tropopause was used in computation of tropospheric columns from sondes and also from collocated

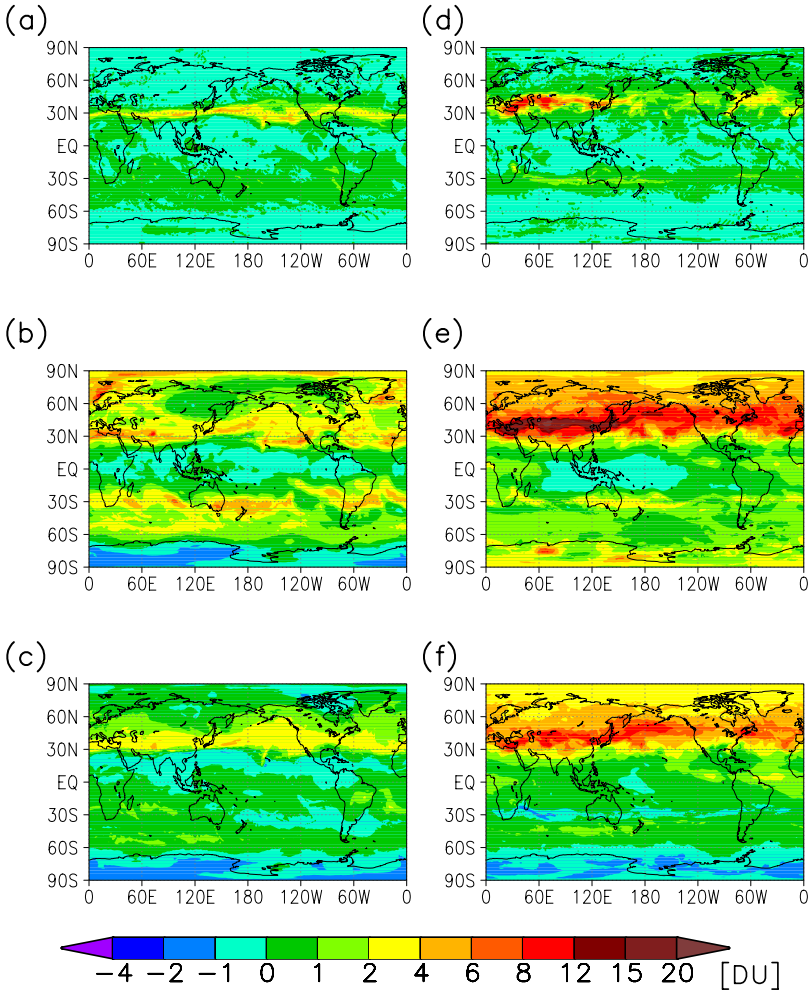

Figure 8. Monthly-mean differences between tropospheric ozone columns in (a–c) February and (d–f) July 2005: $\Omega_{OA} - \Omega_O$ (Figures 8a and 8d), $\Omega_{WMO} - \Omega_O$ (Figures 8b and 8e), and $\Omega_D - \Omega_O$ (Figures 8c and 8f).

model and assimilation profiles. The seasonal evolution of tropospheric ozone and many features of its day-to-day variability that are seen in sondes are reproduced by both the model and the Aura assimilation.

[43] Assimilation of Aura data tends to decrease tropospheric ozone columns compared to the model at high and middle northern latitudes in the winter and spring (e.g., by ~10 DU at Sodankyla in March). This is seen at Sodankyla and Payern from January to May and in December (Figures 10a and 10b). The decrease of tropospheric ozone due to assimilation of Aura data is excessive at Sodankyla in March (Figure 10a). Nevertheless, at Sodankyla and Payern the assimilation is in better overall agreement than the model with the sonde TOC. The RMS differences are lower and the correlations are higher for the assimilation than for the model (Table 3).

[44] In the tropics, the assimilation of Aura data typically increases tropospheric ozone compared to the model tropospheric ozone (Figure 10c and Table 3). This improves the agreement with integrated columns from Southern Hemisphere Additional Ozonesondes (SHADOZ) [*Thompson et al.*, 2003] over South America, the Atlantic, Africa, and the Indian Ocean (Table 3), but also leads to an overestimate of

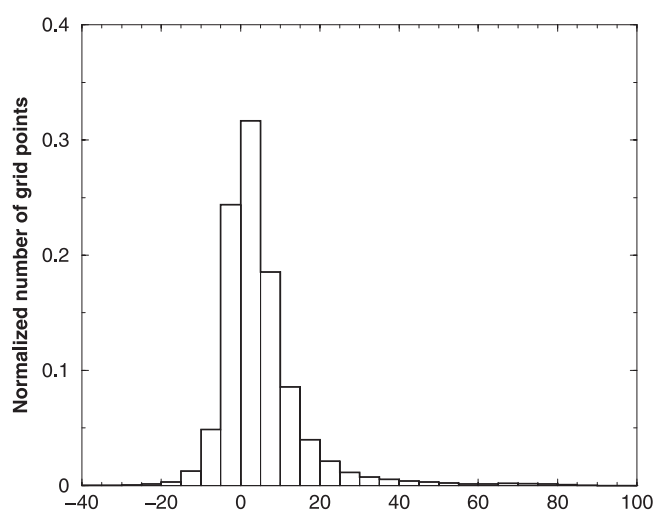

Figure 9. Histogram of $(\Omega_{WMO} - \Omega_O)/\Omega_{WMO}$ in percent in the European region (50°N–80°N, 0°E–20°E) for January to April, November, and December 2005.

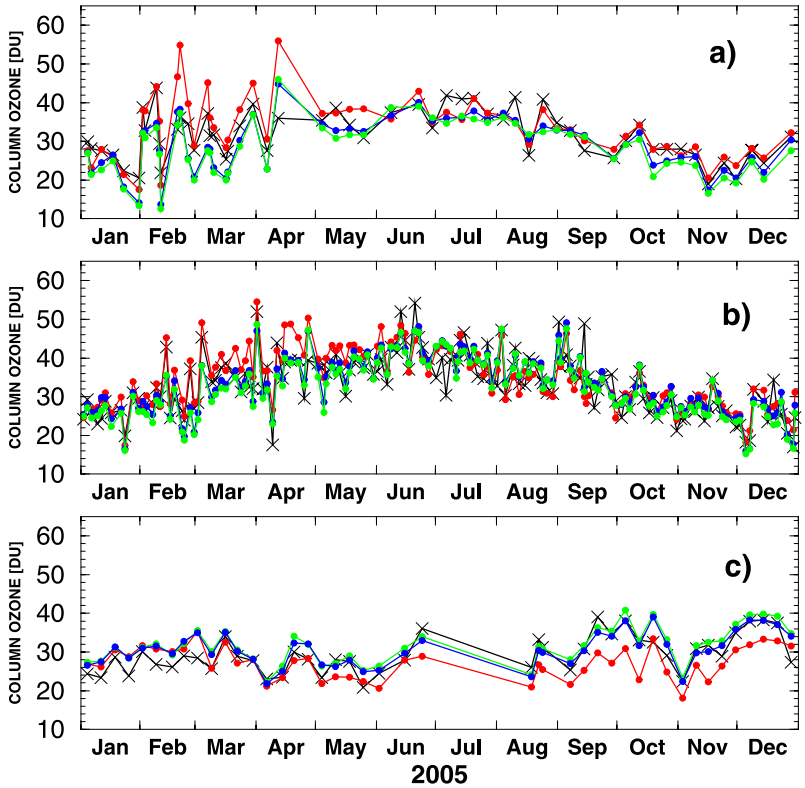

Figure 10. Tropospheric ozone columns at (a) Sodankyla (67.4°N, 26.7°E), (b) Payern (46.8°N, 7°E), and (c) Nairobi (1.3°S, 36.8°E) for year 2005 from ozonesondes (black), model simulation without Aura data (red), Aura assimilation (blue), and Aura assimilation with 50% lower Microwave Limb Sounder (MLS) observation errors (green).

tropospheric ozone over the Pacific (Table 3). For example, at Pago Pago (14.2°S, 189.4°E;) tropospheric ozone from Aura assimilation is higher by 5.52 DU on average than that from the sonde profiles during year 2005. Assimilated tropospheric column at Pago Pago is also higher than model tropospheric column. This is consistent with findings of *Ziemke et al.* [2006] in the tropical Pacific, where tropospheric column residual determined from OMI and MLS data is larger than that simulated by a CTM.

[45] Observed-minus-forecast (O-F) residuals, that is, differences between the incoming data and model forecast of the same variables are routinely computed during the assimilation cycle, and they can provide information about observation error characteristics [e.g., *Stajner et al.*, 2004]. Inspection of zonal means and maps of OMI total ozone column O-F residuals reveals that they are consistent with the changes in the tropospheric ozone columns seen in Figure 10; that is, OMI O-F residuals tend to be positive in the tropics, especially in the Pacific. OMI O-F residuals are often negative outside the tropics, for example, in the Northern Hemisphere in March.

[46] Examples of monthly-mean OMI O-F residuals in the tropics are shown in Figure 11. In January (Figure 11a) the monthly mean of OMI O-Fs is within ±4 DU in most regions, and it exceeds 4 DU in the Indian Ocean near La Reunion (21.1°S, 55.5°E), in the South America, and near 5°S in the Atlantic. The character of OMI-model discrepancies is somewhat different in each of these three regions. At La Reunion model TOCs are lower than those from sondes in January, so positive OMI O-Fs lead to increased TOCs in the assimilation and an improved agreement with sonde TOCs. In the South America (from about 10°S, 280°E to about 5°S, 300°E) mean OMI O-Fs exceed 6 DU; however, this is also a region with frequent clouds where reflectivity is often higher than 15%, so OMI observations are assimilated for fewer than 15 days in January. Data gaps during assimilation are known to often lead to accumulation of model errors and consequently larger O-F residuals. In the Atlantic near 5°S positive OMI O-Fs yield higher tropospheric ozone in the assimilation compared to both the model and the nearby ozonesonde station on the Ascension Island (8°S, 345.6°E). The OMI O-Fs are slightly lower in this region when MLS data are assimilated using lower error specifications providing a tighter constraint on ozone in the lower stratosphere (not shown). Thus, larger OMI O-F in the Atlantic may be an indication of errors in the transport and in the representation of vertical ozone gradients in the lower stratosphere.

[47] In April mean OMI O-Fs are negative over southern Africa, the western Pacific, Australia, and parts of South America (Figure 11b). In contrast, OMI O-Fs are positive over the Indian Ocean, the central and eastern Pacific Ocean, and the region spanning the southern Atlantic Ocean and equatorial Africa. In October OMI O-Fs over South America and Africa exceed 6 DU indicating that ozone production may be stronger than specified in the model. Note that tropospheric ozone columns in the assimilation respond to the OMI O-F residuals. Inspection of monthly

Table 3. Statistics of Tropospheric Ozone Computed Using the WMO Tropopause From Sonde Temperatures[a]

Station Name	Lat., °N	Long., °E	Number of Profiles	Sonde Mean, DU	Sonde-Minus-Model Mean, DU	Sonde-Minus-Assimilation Mean, DU	Model-Sonde RMS Difference, DU	Assimilation-Sonde RMS Difference, DU	Correlation Between Sonde and Model	Correlation Between Sonde and Assimilation
Eureka	80	274	67	27.47	−1.81	2.28	4.46	4.44	0.68	0.69
Ny-Aalesund	79	12	80	30.90	−0.59	3.84	4.23	5.78	0.85	0.80
Resolute	75	265	29	26.31	−1.73	1.96	5.08	4.95	0.60	0.63
Sodankyla	67	27	55	31.51	−1.83	2.47	5.09	4.38	0.80	0.84
Churchill	59	266	27	29.68	−0.30	1.83	4.11	5.17	0.67	0.58
Goose Bay	53	300	52	31.35	−2.68	0.01	5.09	4.11	0.86	0.85
Legionowo	52	21	65	34.33	−2.36	1.47	4.60	4.13	0.84	0.85
De Bilt	52	5	54	34.88	−4.01	−1.18	5.17	3.61	0.90	0.89
Kelowna	50	241	32	30.44	−1.17	1.51	4.44	3.78	0.74	0.81
Bratts Lake	50	255	39	30.31	−2.83	−1.70	5.08	4.12	0.81	0.85
Payern	47	7	148	33.33	−1.42	−0.21	4.58	3.88	0.83	0.86
Egbert	44	280	50	35.91	−2.74	−1.50	5.92	4.62	0.88	0.92
Barajas	40	356	39	34.27	−2.31	−1.68	5.90	4.41	0.63	0.80
Wallops Island	38	285	65	40.82	−2.04	−2.11	5.81	4.31	0.85	0.93
Isfahan	33	52	13	34.67	2.11	2.43	6.94	5.45	0.57	0.81
Hong Kong	22	114	46	39.37	4.15	0.63	6.22	3.55	0.82	0.90
Paramaribo	6	305	34	29.99	3.28	−1.10	6.60	4.41	0.29	0.69
Sepang	3	102	23	26.47	2.20	−1.08	3.46	3.00	0.84	0.87
Nairobi	−1	37	44	29.38	2.19	−1.31	4.68	2.92	0.57	0.84
Malindi	−3	40	19	35.52	6.69	2.60	8.11	4.48	0.55	0.76
Natal	−5	325	23	32.05	1.64	−2.08	6.78	4.68	0.65	0.88
Ascension Island	−8	346	41	38.76	4.93	−1.63	8.68	6.81	0.59	0.66
Pago Pago	−14	189	29	19.62	−0.23	−5.52	4.05	7.20	0.59	0.63
La Réunion	−21	55	36	35.71	4.13	−0.80	7.18	4.74	0.78	0.86
Irene	−26	28	31	35.75	3.60	0.49	5.42	3.64	0.84	0.86
Neumayer	−71	352	79	22.50	0.99	0.45	3.17	3.59	0.94	0.90

[a]Mean from sondes, mean difference between sondes and the model simulation without Aura data, and mean difference between sondes and the assimilation of Aura data for year 2005 are given in columns 5, 6, and 7, respectively. Root-mean-square (RMS) difference between model and sondes is given in column 8, and the RMS difference between Aura assimilation and sondes is given in column 9. Correlations between sondes and the model and correlations between sondes and the assimilation are given in columns 10 and 11, respectively.

differences in tropospheric ozone columns between Aura assimilation and model simulations indicates similar patterns to those seen in OMI O-F residual maps in Figure 11: tropospheric columns increase the most in the Aura assimilation compared to the model simulation in the regions where OMI O-F residuals are the largest. A persistent drought in the Amazon basin lead to increased biomass burning in October 2005 [*Zeng et al.*, 2007]. The model uses climatological biomass burning emissions, and thus underestimates ozone production in this region. Assimilation of Aura OMI data increases the tropospheric ozone by about 10 DU in this region and greatly improves the agreement with ozonesondes in Natal and Paramaribo during September–December.

[48] Positive OMI O-Fs are seen in monthly means from May to December 2005 in the western and central Pacific (see, e.g., July and October in Figures 11c and 11d). The assimilation of OMI data increases total ozone columns there, while MLS data are constraining stratospheric profiles, leading to accumulation of ozone in the troposphere. This is consistent with the overestimation of the TOC in the assimilation at Pago Pago (Table 3), which was found in the comparison of Aura assimilation with ozonesondes from 25 March to the end of the year. Even though this could implicate OMI data as the source of differences between TOC from ozonesondes and the Aura assimilation, errors in other components of the assimilation system (e.g., MLS data and transport of ozone in the model) as well as the quality of ozonesonde data need to be considered.

[49] The residual circulation is known to be overly strong in the GEOS-4 analyses [*Pawson et al.*, 2007], which leads to a deficit in stratospheric ozone in the tropics and an excess in the extra-tropics. The MLS O-F residuals between ~1 and 50 hPa, and the analysis increments (i.e., changes in the ozone field due to the assimilation of observational data) are consistent with this scenario. We note in passing that horizontal mixing across the subtropical barrier does not seem to be excessive in GEOS-4.0.3 [cf. *Bloom et al.*, 2005], as it was in earlier versions of the transport [*Tan et al.*, 2004]. With an earlier version of the transport (from GEOS-4.0.1), *Wargan et al.* [2005] found that ozone analysis increments due to assimilation of data from MIPAS limb sounding instrument were systematically counteracting the reduction of the ozone gradients, which was caused by an excessive mixing across the subtropical barrier.

[50] Version 1.5 of the MLS data is known to be biased high in the UTLS. The lowest MLS level being assimilated is near 215 hPa. In the tropics this level is usually in the upper troposphere, and in the extratropics it is often in the lower stratosphere. Thus, MLS data could contribute directly to higher tropical tropospheric ozone. By increasing stratospheric ozone in the extratropics, for a fixed OMI total column, they could indirectly cause lower tropospheric column residual. Note that even though MLS data are assimilated at 215 hPa, the error specifications are large (e.g., ~20%–50% in the tropics), so that analyses are not strongly drawn to MLS data at that level. In order to separate the impact of MLS data we assimilated Aura data in another experiment in which MLS observation error standard devia-

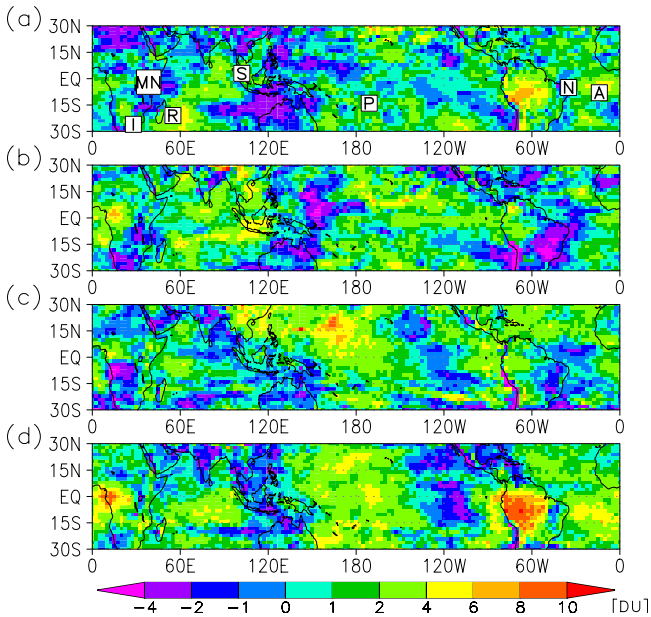

Figure 11. Maps of monthly means of Ozone Monitoring Instrument (OMI) observed-minus-forecast (O-F) residuals (Dobson Units, DU) in the tropics for (a) January 2005, (b) April 2005, (c) July 2005, and (d) October 2005. Positive values indicate that OMI observations are larger than the model forecast of total column ozone. Locations of eight SHADOZ stations are marked in Figure 11a: Irene (I), Malindi and Nairobi (M, N), La Réunion (R), Sepang (S), Pago Pago (P), Natal (N), and Ascension Island (A).

tions were specified as 50% lower. The impact of this change is about 1 DU on the tropospheric column, decreasing it in the northern high and middle latitudes in winter and spring. Impacts in the tropics vary with season and location: increases are mostly found close to the equator, and decreases toward the subtropics. These changes are too small to explain the biases shown in Figure 10.

[51] Retrieved OMI total ozone columns incorporate prior information provided by an ozone climatology, which varies with latitude and time, but is zonally symmetric [*McPeters et al.*, 2007]. However, there is pronounced zonal variability in tropospheric ozone in the tropics with higher ozone in the Atlantic than in the Pacific basin [e.g., *Thompson et al.*, 2003]. This wave one feature in the tropospheric ozone may lead to overestimation of ozone in the Pacific. Indeed, *Thompson et al.* [2007a] found that version 8 retrievals of total ozone columns from the Earth Probe TOMS instrument are typically higher than the total ozone columns retrieved from the Dobson instrument and from integration of sonde profiles at Pago Pago, with larger differences against the latter. Note that version 8 TOMS retrievals are very similar to the OMI total ozone retrievals used here.

[52] There are also known issues with the ozonesonde data at Pago Pago [*Thompson et al.*, 2007a]. At this station, Science Pump Model 6A sondes are used with a 2% KI unbuffered solution. Even after a pump correction factor is applied to the sonde measurements, reported ozone data are estimated to be about 9% to 10% lower than the true values between the surface and 10 km altitude. These estimates were obtained by simulating the flight conditions in a chamber and comparing with more accurate measurements. In addition, total ozone obtained from sonde measurements is by 7%–8% lower than that from a collocated Dobson spectrophotometer between the end of 25 March and 31 December 2005 (S. Oltmans, personal communication, 2007). If a uniform 10% correction were applied to the Pago Pago sonde data, the RMS difference between TOCs from the sondes and from the model or assimilation experiments would be as follows: 4.55 DU for the model, 5.89 DU for the Aura assimilation, and 5.59 DU for the Aura assimilation with 50% reduced MLS error specifications. Thus, the RMS differences would increase for the model (4.55 DU compared to 4.05 DU in Table 3), and decrease for the Aura assimilation (5.89 DU compared to 7.20 DU in Table 3).

[53] The TOCs from the Aura assimilation were found to reproduce the annual cycle and some of the day-to-day variability in comparison with ozonesondes (Figure 10). The RMS differences in the TOCs against the ozonesonde data are reduced in the assimilation of Aura data to about 2.9–7.4 DU compared to those from model simulation, which range from 3.2 DU to 8.7 DU (Table 3). The correlation with sonde tropospheric columns is also higher for the assimilation of Aura data (0.58–0.93) than for the model run (0.29–0.93). OMI O-F residuals provide a quantitative measure of data-model discrepancies, which are later reflected in the impacts of Aura data on the estimated ozone columns. Using the Pacific example, it was illustrated that interplay between different components of the assimilations system needs to be considered when evaluating impacts of assimilation on the TOCs. Furthermore, in the evaluation of the quality of the TOC estimates, the biases in the comparative data needs to be considered as well (e.g., for Pago Pago ozonesondes).

[54] Annual mean TOC for year 2005 that was determined using the dynamical definition of the tropopause is shown in Figure 12a [cf. *Schoeberl et al.*, 2007]. The highest TOCs are seen from the Mediterranean to India, over eastern China, the eastern United States and southern Africa, with high TOCs extending downstream over neighboring oceans. In the Northern Hemisphere over the oceans, the high tropospheric ozone columns are centered about 30°N. Low TOCs are seen over elevated terrain: the Himalayas, the Andes, the Rockies, Antarctica, and Greenland. When mean ozone mixing ratio between the surface and the dynamical tropopause is considered (Figure 12b), the maxima are more confined to the continents. The highest mixing ratios over the northern oceans are between about 30°N to 40°N. The highest tropospheric mean mixing ratio is over the Tibetan Plateau. This is the region of the highest STE [*Hsu et al.*, 2005] and also with substantial differences between tropospheric ozone columns defined using dynamical tropopause and the ozone tropopause (Figures 8c and 8f). If the WMO (ozone) definition of the tropopause is used, the annual average tropospheric ozone mixing ratio increases (decreases) around 30°N and 30°S (not shown).

7. Discussion and Conclusions

[55] Ozone data from Aura MLS and OMI were assimilated into the GEOS-4 GCM to construct global three-

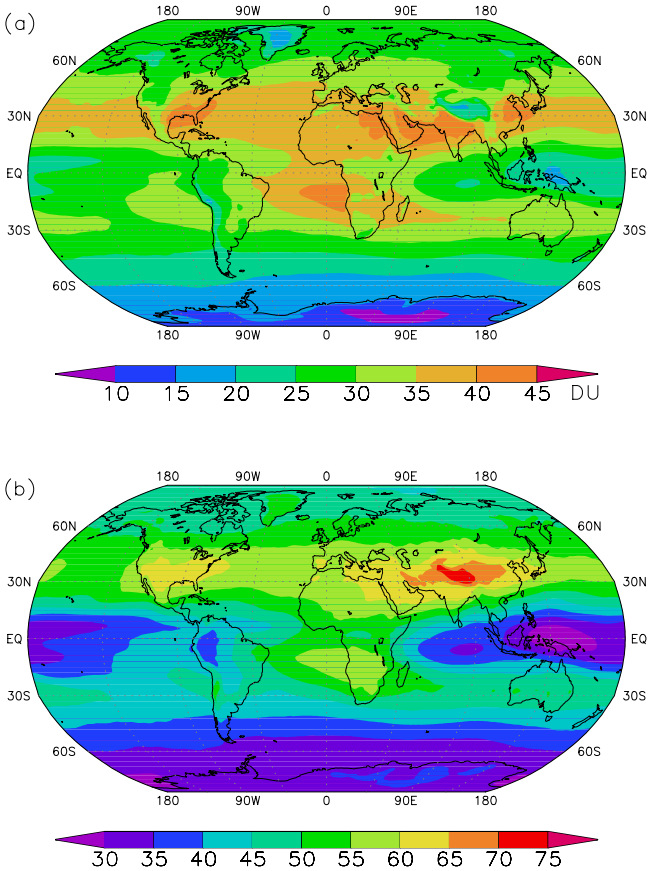

Figure 12. (a) Mean tropospheric ozone columns (TOC) (DU) for year 2005 determined using dynamical definition of the tropopause. (b) Mean tropospheric ozone mixing ratio (ppbv) for year 2005 determined using dynamical definition of the tropopause.

dimensional ozone fields every 3 hours. Assimilation of MLS data improves representation of the stratospheric ozone, by counteracting ozone changes due to overstrong residual circulation in the model, and bringing the assimilated ozone closer to independent data in the lower stratosphere (e.g., Figure 2b) as in the work of *Wargan et al.* [2005] and *Jackson* [2007]. Comparisons with independent ozonesonde and MOZAIC data indicate a slight overestimation of ozone near 200 hPa in the Aura assimilation (e.g., 8% against ozonesondes in Figure 2b). Tropospheric ozone columns from Aura assimilation reproduce the seasonal cycle and much of the day-to-day variability in the ozonesonde data (Figure 10). The validation indicates that ozone in the upper troposphere and stratosphere is represented quite successfully in this assimilation, with a somewhat high bias in the upper troposphere and other differences associated with poor alignment of the tropopause in the meteorological analyses compared that that in the observations. Overall, the quality of the assimilated ozone profile in the vicinity of the tropopause is adequate for studies of TOC to be meaningful.

[56] The sensitivity of tropospheric ozone to different definitions of the tropopause was investigated using global assimilated ozone and meteorological fields from GEOS-4. Our findings are consistent with the study of *Bethan et al.* [1996], which was done using in situ ozonesonde data in a small region. In the northern middle latitudes Ω_O tends to be lower by ~10% than Ω_{WMO} (Figure 6b), because the ozone-defined tropopause is lower than the WMO-defined tropopause by ~1 km (Figure 6a). Occasionally, Ω_O can be lower than Ω_{WMO} by ~80% (Figure 9), especially on the poleward side of strong wind jets in the UTLS (Figure 7). Consequently, the distribution and the magnitude of differences between tropospheric ozone columns due to different tropopause definitions vary by season. Larger differences are often found in the vicinity of the subtropical jets, sometimes with pronounced zonal asymmetry (Figure 8). Further study of the impacts of tropopause on tropospheric columns is warranted. Our comparisons indicate that using the tropopause with the lowest altitude among WMO, dynamical, and ozone definitions may be best suited for air quality applications. This would avoid misinterpretation of lower stratospheric ozone or reversible intrusions of stratospheric ozone in the upper troposphere as enhanced tropospheric ozone columns.

[57] TOC derived from the assimilated ozone leads to reasonable estimates in comparison with ozonesondes in the middle latitudes, in the tropical Atlantic, and the Indian Ocean (Figure 10). Excessively high tropospheric ozone in the tropical Pacific and excessively low tropospheric ozone in the northern high latitudes during winter and spring could be caused indirectly by the overly strong residual circulation in the model. However, altitude-dependent biases in MLS, in addition to regional and seasonal biases in OMI data may be contributing as well. For example, tropospheric ozone in the northern high latitudes in the winter is closer to that from sondes when MLS data are assimilated using MLS precision as observation error, compared to 50% lower MLS observation error. In contrast, 50% lower specification of MLS errors improves tropospheric ozone columns at subtropical locations in the tropical Pacific: this indicates that transport errors or OMI data may be responsible for biases there. For example, OMI retrievals could be biased high owing to their use of a zonally independent a priori, even though tropical tropospheric ozone is known to be lower in the Pacific than in the Atlantic region. Another source of the high bias in tropospheric ozone may be the selection of OMI data: they are assimilated only in the cloud-free regions (where reflectivity at 331 nm is less than 15%) where photochemical ozone production is stronger.

[58] This study has demonstrated that substantial information about ozone in the tropopause region can be obtained by assimilating high-quality limb-sounder data. It has also shown, with caveats, the ability of assimilation to provide useful information on the global distribution of tropospheric ozone columns, along with details on vertical structure provided by the GCM, which is consistent with earlier studies on assimilation of constituent data an the troposphere [e.g., *Elbern and Schmidt*, 2001; *Pradier et al.*, 2006]. There are several possible refinements that we plan to investigate. First, in order to improve the understanding of how well tropospheric ozone can be constrained by assimilation of Aura data, we intend to use later versions of MLS and OMI retrievals, as they become available (e.g., collection 3 for OMI [*Dobber et al.*, 2008]). For instance, MLS version 2.2 MLS data have a less biased representation of UTLS ozone than the version 1.5 MLS retrievals

used here [see *Froidevaux et al.*, 2008; *Jiang et al.*, 2007; *Livesey et al.*, 2008]. There is also the possibility of using the DOAS total ozone retrieval from OMI. The accuracies of collection 3 DOAS and OMTO3 total ozone data are comparable [*Kroon et al.*, 2008]. A potential advantage of the DOAS algorithm is the use of cloud pressure measured by OMI using O2-O2 cloud detection method [*Accareta et al.*, 2004], which could be incorporated in the assimilation of OMI data in cloudy regions. Second, we plan to exploit the high spatial resolution of OMI data by examining the impacts of relaxing the spatial averaging, which will require a careful assessment of the observation error covariance, especially in cloudy regions. Third, assimilation of ozone information derived from the Tropospheric Emission Sounder (TES) instrument, which provides tropospheric ozone retrievals along with appropriate averaging kernels, even under cloudy conditions [*Kulawik et al.*, 2006] will be investigated. These are examples of how we expect to exploit the variety of information about ozone contained in the suite of instruments on Aura to better improve our understanding of tropospheric ozone. The results shown in this study support the notion that combining information from different types of sensors by data assimilation is a useful method for enhancing the value of the individual types of retrieval, with the caveat that different characteristics of the various data types and the model must be considered when interpreting features in the assimilated products.

[59] **Acknowledgments.** This work was supported by NASA's Atmospheric Chemistry Modeling and Analysis Program. Work at the Jet Propulsion Laboratory, California Institute of Technology, was carried out under a contract with the National Aeronautics and Space Administration. The assimilation was performed using NASA's High-Performance Computing resources. The Dutch-Finnish-built OMI instrument is part of the NASA EOS-Aura satellite payload. The OMI project is managed by NIVR and KNMI in the Netherlands. We thank the OMI International Science Team for the satellite data used in this study. OMI ozone OMTO3 data were obtained from the NASA Goddard Earth Sciences (GES) Data and Information Services Center (DISC), home of the GES Distributed Active Archive Center (DAAC). Ozonesonde data were obtained from the Aura Validation Data Center and from the Envisat Calibration and Validation Database. The authors acknowledge for their strong support the European Commission, Airbus, and the airlines (Lufthansa, Austrian, and Air France) who since 1994 have carried free of charge the MOZAIC equipment and performed the maintenance. MOZAIC is supported by INSU-CNRS (Institut National des Sciences de l'Univers–Centre National de la Recherche Scientifique, France), Météo-France, and FZJ (Forschungszentrum Jülich, Germany). I.S. thanks Stephen Cohn, Matthew Hitchman, and Marek Rogal for useful discussions.

References

Accareta, J. R., J. F. De Haan, and P. Stammes (2004), Cloud pressure retrievalusing the O2-O2 absorption band at 477 nm", *J. Geophys. Res.*, *109*, D05204, doi:10.1029/2003JD003915.

Bethan, S., G. Vaughan, and S. Reed (1996), A comparison of ozone and thermal tropopause heights and the impact of tropopause definition on quantifying the ozone content of the tropopause, *Q. J. R. Meteorol. Soc.*, *122*, 929–944.

Bey, I., D. J. Jacob, R. M. Yantosca, J. A. Logan, B. D. Field, A. M. Fiore, Q. Li, H. Y. Liu, L. J. Mickley, and M. G. Schultz (2001), Global modeling of tropospheric chemistry with assimilated meteorology: Model description and evaluation, *J. Geophys. Res.*, *106*, 23,073–23,096.

Birner, T., D. Sankey, and T. G. Shepherd (2006), The tropopause inversion layer in models and analyses, *Geophys. Res. Lett.*, *33*, L14804, doi:10.1029/2006GL026549.

Bloom, S. C., et al. (2005), The Goddard Earth Observing System Data Assimilation System, GEOS DAS version 4.0.3: Documentation and validation, *NASA Tech. Memo*., *NASA TM-2005-104606*, vol. 26, 166 pp., NASA Goddard Space Flight Cent., Greenbelt, Md.

Cohn, S. E., A. da Silva, J. Guo, M. Sienkiewicz, and D. Lamich (1998), Assessing the effects of data selection with the DAO Physical-Space Statistical Analysis System, *Mon. Weather Rev.*, *126*, 2913–2926.

Dobber, M. R., Q. Kleipool, R. Dirksen, P. Levelt, G. Jaross, S. Taylor, T. Kelly, L. E. Flynn, G. Leppelmeier, and N. Rozemeijer (2008), Validation of Ozone Monitoring Instrument level 1b data products, *J. Geophys. Res.*, *113*, D15S06, doi:10.1029/2007JD008665.

Douglass, A. R., C. J. Weaver, R. B. Rood, and L. Coy (1996), A three-dimensional simulation of the ozone annual cycle using winds from a data assimilation system, *J. Geophys. Res.*, *101*(D1), 1463–1474.

Duncan, B. N., J. A. Logan, A. C. Staudt, R. Yevich, and J. A. Logan (2003), Interannual and seasonal variability of biomass burning emissions constrained by satellite observations, *J. Geophys. Res.*, *108*(D2), 4100, doi:10.1029/2002JD002378.

Elbern, H., and H. Schmidt (2001), Ozone episode analysis by four-dimensional variational chemistry data assimilation, *J. Geophys. Res.*, *106*(D4), 3569–3590.

Eskes, H. J., P. van Velthoven, P. J. M. Valks, and H. M. Kelder (2003), Assimilation of GOME total ozone satellite observations in a three-dimensional tracer transport model, *Q. J. R. Meteorol. Soc.*, *129*, 1663–1681.

Froidevaux, L., et al. (2006), Early validation analyses of atmospheric profiles from EOS MLS on the Aura satellite, *IEEE Trans. Geosci. Remote Sens.*, *44*, 1106–1112.

Froidevaux, L., et al. (2008), Validation of Aura Microwave Limb Sounder stratospheric ozone measurements, *J. Geophys. Res.*, *113*, D15S20, doi:10.1029/2007JD008771.

Gaspari, G., S. E. Cohn, J. Guo, and S. Pawson (2006), Construction and application of covariance functions with variable length fields, *Q. J. R. Meteorol. Soc.*, *132*, 1815–1838.

Hadjinicolaou, P., J. A. Pyle, M. P. Chipperfield, and J. A. Kettleborough (1997), Effect of interannual meteorological variability on mid-latitude O_3, *Geophys. Res. Lett.*, *24*(23), 2993–2996.

Hoerling, M. P., T. K. Schaack, and A. J. Lenzen (1991), Global objective tropopause analysis, *Mon. Weather Rev.*, *119*, 1816–1831.

Holton, J. R., P. H. Haynes, M. E. McIntyre, A. R. Douglass, R. B. Rood, and L. Pfister (1995), Stratosphere-troposphere exchange, *Rev. Geophys.*, *33*, 403–439.

Hsu, J., M. J. Prather, and O. Wild (2005), Diagnosing the stratosphere-to-troposphere flux of ozone in a chemistry transport model, *J. Geophys. Res.*, *110*, D19305, doi:10.1029/2005JD006045.

Hudman, R. C., et al. (2007), Surface and lightning sources of nitrogen oxides over the United States: Magnitudes, chemical evolution, and outflow, *J. Geophys. Res.*, *112*, D12S05, doi:10.1029/2006JD007912.

Jackson, D. (2007), Assimilation of EOS MLS ozone observations in the Met Office Data Assimilation System, *Q. J. R. Meteorol. Soc.*, *133*, 1771–1788.

Jiang, Y. B., et al. (2007), Validation of Aura Microwave Limb Sounder ozone by ozonesonde and lidar measurements, *J. Geophys. Res.*, *112*, D24S34, doi:10.1029/2007JD008776.

Kistler, R., et al. (2001), The NCEP-NCAR 50-year reanalysis: Monthly means CD-ROM and documentation, *Bull. Am. Meteorol. Soc.*, *82*, 247–267.

Kroon, M., J. P. Veefkind, M. Sneep, R. D. McPeters, P. K. Bhartia, and P. Levelt (2008), Comparing OMI-TOMS and OMI-DOAS total ozone column data, *J. Geophys. Res.*, doi:10.1029/2007JD008798, in press.

Kulawik, S. S., J. Worden, A. Eldering, K. Bowman, M. Gunson, G. B. Osterman, L. Zhang, S. A. Clough, M. W. Shephard, and R. Beer (2006), Implementation of cloud retrievals for Tropospheric Emission Spectrometer (TES) atmospheric retrievals: 1. Description and characterization of errors on trace gas retrievals, *J. Geophys. Res.*, *111*, D24204, doi:10.1029/2005JD006733.

Lamarque, J.-F., B. V. Khattatov, and J. C. Gille (2002), Constraining tropospheric ozone column through data assimilation, *J. Geophys. Res.*, *107*(D22), 4651, doi:10.1029/2001JD001249.

Levelt, P. F., et al. (2006), The Ozone Monitoring Instrument, *IEEE Trans. Geophys. Remote Sens.*, *44*(5), 1093–1101.

Lin, S.-J. (2004), A "vertically Lagrangian" finite-volume dynamical core for global models, *Mon. Weather Rev.*, *132*(10), 2293–2307.

Lin, S.-J., and R. B. Rood (1996), Multidimensional flux-form semi-Lagrangian transport schemes, *Mon. Weather Rev.*, *124*, 2046–2070.

Livesey, N. J., et al. (2008), Validation of Aura Microwave Limb Sounder O3 and CO observations in the upper troposphere and lower stratosphere, *J. Geophys. Res.*, *113*, D15S02, doi:10.1029/2007JD008805.

Logan, J. A., D. B. A. Jones, I. A. Megretskaia, S. J. Oltmans, B. J. Johnson, H. Vömel, W. J. Randel, W. Kimani, and F. J. Schmidlin (2003), Quasibiennial oscillation in tropical ozone as revealed by ozonesonde and satellite data, *J. Geophys. Res.*, *108*(D8), 4244, doi:10.1029/2002JD002170.

Marenco, A., et al. (1998), Measurement of ozone and water vapor by Airbus in-service aircraft: The MOZAIC airborne program, An overview, *J. Geophys. Res.*, *103*(D19), 25,631–25,642.

McPeters, R. D., G. J. Labow, and J. A. Logan (2007), Ozone climatological profiles for satellite retrieval algorithms, *J. Geophys. Res.*, *112*, D05308, doi:10.1029/2005JD006823.

McPeters, R. D., et al. (2008), Validation of the Aura Ozone Monitoring Instrument total column ozone product, *J. Geophys. Res.*, *113*, D15S14, doi:10.1029/2007JD008802.

Pan, L. L., W. J. Randel, B. L. Gary, M. J. Mahoney, and E. J. Hintsa (2004), Definitions and sharpness of the extratropical tropopause: A trace gas perspective, *J. Geophys. Res.*, *109*, D23103, doi:10.1029/2004JD004982.

Park, R. J., D. J. Jacob, B. D. Field, R. M. Yantosca, and M. Chin (2004), Natural and transboundary pollution influences on sulfate-nitrate-ammonium aerosols in the United States: Implications for policy, *J. Geophys. Res.*, *109*, D15204, doi:10.1029/2003JD004473.

Pawson, S., I. Stajner, S. R. Kawa, H. Hayashi, W.-W. Tan, J. E. Nielsen, Z. Zhu, L.-P. Chang, and N. J. Livesey (2007), Stratospheric transport using 6-h-averaged winds from a data assimilation system, *J. Geophys. Res.*, *112*, D23103, doi:10.1029/2006JD007673.

Pickering, K. E., A. M. Thompson, J. R. Scala, W. Tai, R. R. Dickerson, and J. Simpson (1992), Free tropospheric ozone production following entrainment of urban plumes into deep convection, *J. Geophys. Res.*, *97*(D16), 17,985–18,000.

Pradier, S., J. L. Attie, M. Chong, J. Escobar, V. H. Peuch, J. F. Lamarque, B. Khattatov, and D. Edwards (2006), Evaluation of 2001 springtime CO transport over West Africa using MOPITT CO measurements assimilated in a global chemistry transport model, *Tellus, Ser. B*, *58*(3), 163–176.

Price, C., and D. Rind (1992), A simple lightning parameterization for calculating global lightning distributions, *J. Geophys. Res.*, *97*, 9919–9933.

Reichler, T., M. Dameris, and R. Sausen (2003), Determining the tropopause height from gridded data, *Geophys. Res. Lett.*, *30*(20), 2042, doi:10.1029/2003GL018240.

Schoeberl, M. R. (2004), Extratropical stratosphere-troposphere mass exchange, *J. Geophys. Res.*, *109*, D13303, doi:10.1029/2004JD004525.

Schoeberl, M. R., et al. (2006), Overview of the EOS Aura mission: Experiment, *IEEE Trans. Geosci. Remote Sens.*, *44*(5), 1066–1074.

Schoeberl, M. R., et al. (2007), A trajectory-based estimate of the tropospheric ozone column using the residual method, *J. Geophys. Res.*, *112*, D24S49, doi:10.1029/2007JD008773.

Sparling, L. C., and J. T. Bacmeister (2001), Scale dependence of tracer microstructure: PDFs, intermittency and the dissipation scale, *Geophys. Res. Lett.*, *28*(14), 2823–2826.

Stajner, I., and K. Wargan (2004), Antarctic stratospheric ozone from the assimilation of occultation data, *Geophys. Res. Lett.*, *31*, L18108, doi:10.1029/2004GL020846.

Stajner, I., L. P. Riishøjgaard, and R. B. Rood (2001), The GEOS ozone data assimilation system: Specification of error statistics, *Q. J. R. Meteorol. Soc.*, *127*, 1069–1094.

Stajner, I., N. Winslow, R. B. Rood, and S. Pawson (2004), Monitoring of observation errors in the assimilation of satellite ozone data, *J. Geophys. Res.*, *109*, D06309, doi:10.1029/2003JD004118.

Stajner, I., K. Wargan, L.-P. Chang, H. Hayashi, S. Pawson, and H. Nakajima (2006), Assimilation of ozone profiles from the Improved Limb Atmospheric Spectrometer–II: Study of Antarctic ozone, *J. Geophys. Res.*, *111*, D11S14, doi:10.1029/2005JD006448.

Tan, W. W., M. A. Geller, S. Pawson, and A. da Silva (2004), A case study of excessive subtropical transport in the stratosphere of a data assimilation system, *J. Geophys. Res.*, *109*, D11102, doi:10.1029/2003JD004057.

Thompson, A. M., et al. (2003), Southern Hemisphere Additional Ozonesondes (SHADOZ) 1998–2000 tropical ozone climatology: 1. Comparison with Total Ozone Mapping Spectrometer (TOMS) and ground-based measurements, *J. Geophys. Res.*, *108*(D2), 8238, doi:10.1029/2001JD000967.

Thompson, A. M., J. C. Witte, H. G. J. Smit, S. J. Oltmans, B. J. Johnson, V. W. J. H. Kirchhoff, and F. J. Schmidlin (2007a), Southern Hemisphere Additional Ozonesondes (SHADOZ) 1998–2004 tropical ozone climatology: 3. Instrumentation, station variability, and evaluation with simulated flight profiles, *J. Geophys. Res.*, *112*, D03304, doi:10.1029/2005JD007042.

Thompson, A. M., et al. (2007b), Intercontinental Chemical Transport Experiment Ozonesonde Network Study (IONS) 2004: 1. Summertime upper troposphere/lower stratosphere ozone over northeastern North America, *J. Geophys. Res.*, *112*, D12S12, doi:10.1029/2006JD007441.

Thouret, V., A. Marenco, J. A. Logan, P. Nédélec, and C. Grouhel (1998a), Comparisons of ozone measurements from the MOZAIC airborne program and the ozone sounding network at eight locations, *J. Geophys. Res.*, *103*(D19), 25,695–25,720.

Thouret, V., A. Marenco, P. Nédélec, and C. Grouhel (1998b), Ozone climatologies at 9–12 km altitude as seen by the MOZAIC airborne program between September 1994 and August 1996, *J. Geophys. Res.*, *103*(D19), 25,653–25,680.

Veefkind, J. P., J. F. de Haan, E. J. Brinksma, M. Kroon, and P. F. Levelt (2006), Total ozone from the Ozone Monitoring Instrument (OMI) using the DOAS technique, *IEEE Trans. Geosci. Remote Sens.*, *44*(5), 1239–1244.

Wang, H. J., D. M. Cunnold, L. W. Thomason, J. M. Zawodny, and G. E. Bodeker (2002), Assessment of SAGE version 6.1 ozone data quality, *J. Geophys. Res.*, *107*(D23), 4691, doi:10.1029/2002JD002418.

Wargan, K., I. Stajner, S. Pawson, R. B. Rood, and W.-W. Tan (2005), Monitoring and assimilation of ozone data from the Michelson Interferometer for passive atmospheric sounding, *Q. J. R. Meteorol. Soc.*, *131*, 2713–2734, doi:10.1256/qj.04.184.

Waters, J. W., et al. (2006), The Earth Observing System Microwave Limb Sounder (EOS MLS) on the Aura satellite, *IEEE Trans. Geosci. Remote Sens.*, *44*, 1075–1092.

Zahn, A., et al. (2000), Identification of extratropical two-way troposphere-stratosphere mixing based on CARIBIC measurements of O_3, CO, and ultrafine particles, *J. Geophys. Res.*, *105*(D1), 1527–1536.

Zeng, N., J. Yoon, J. Marengo, A. Subamaniam, C. Nobre, A. Mariotti, and J. D. Neelin (2007), Causes and impact of the 2005 Amazon drought, *Environ. Res. Lett.*, *3*, 014002, doi:10.1088/1748-9326/3/1/014002.

Ziemke, J. R., S. Chandra, B. N. Duncan, L. Froidevaux, P. K. Bhartia, P. F. Levelt, and J. W. Waters (2006), Tropospheric ozone determined from Aura OMI and MLS: Evaluation of measurements and comparison with the Global Modeling Initiative's Chemical Transport Model, *J. Geophys. Res.*, *111*, D19303, doi:10.1029/2006JD007089.

S. B. Andersen, Danish Meteorological Institute, DK-2100 Copenhagen, Denmark.

L.-P. Chang and K. Wargan, Science Applications International Corporation, Beltsville, MD 20705, USA.

L. Froidevaux and N. Livesey, Jet Propulsion Laboratory, Pasadena, CA 91109, USA.

H. Hayashi, Goddard Earth Sciences and Technology Center, University of Maryland, Baltimore County, Baltimore, MD 21228, USA.

R. C. Hudman, Atmospheric Chemistry Modeling Group, Harvard University, Cambridge, MA 02138, USA.

G. König-Langlo, Alfred Wegener Institute for Polar and Marine Research, Postfach 120161, D-27515 Bremerhaven, Germany.

P. F. Levelt, Royal Dutch Meteorological Institute, KS/AK, 3730 AE, De Bilt, Netherlands.

S. Pawson, Global Modeling and Assimilation Office, NASA Goddard Space Flight Center, Greenbelt, MD 20771, USA.

F. J. Schmidlin, NASA GSFC, Wallops Flight Facility, Wallops Island, VA 23337, USA.

I. Stajner, Noblis, Incorporated, 3150 Fairview Park Drive South, M.S. F540, Falls Church, VA 22042-4519, USA. (ivanka.stajner@noblis.org)

R. Stübi, Aerological Station Payerne, P.O. Box 316, CH-1530, MeteoSwiss, Payerne, Switzerland.

D. W. Tarasick, Air Quality Research Division, Environment Canada, Downsview, ON, M3H 5T4 Canada.

A. M. Thompson, Department of Meteorology, Pennsylvania State University, University Park, PA 16802, USA.

J. C. Witte, Science Systems and Applications Inc., Lanham, MD 20706, USA.

M. Yela, Instituto Nacional de Tecnica Aeroespacial, Carretera de Ajalvir km 4, E-28850, Torrejón de Ardoz, Madrid, Spain.